5. McWilliams, J. C. Modelling the oceanic general circulation. *Annu. Rev. Fluid. Mech.* **28,** 215–248 (1996).
6. Walin, G. The thermohaline circulation and the control of ice ages. *Palaeogeogr. Palaeoclimatol. Palaeoecol.* **50,** 323–332 (1985).
7. Marotzke, J., Welander, P. & Willebrand, J. Instability and multiple steady states in a meridional-plane model of the thermohaline circulation. *Tellus A* **40,** 162–172 (1988).
8. Mikolajewicz, U. & Maier-Reimer, E. Mixed boundary conditions in ocean general circulation models and their influence on the stability of the model's conveyor belt. *J. Geophys. Res.* **99,** 22633–22644 (1994).
9. Brass, G. W., Southam, J. R. & Peterson, W. H. Warm saline bottom water in the ancient ocean. *Nature* **296,** 620–623 (1982).
10. Toggweiler, J. R. *et al.* Reply. *J. Phys. Oceanogr.* **26,** 1106–1110 (1996).
11. Bryan, F. High-latitude salinity effects and interhemispheric thermohaline circulations. *Nature* **323,** 301–304 (1986).
12. Weaver, A. J., Sarachick, E. S. & Marotzke, J. Freshwater flux forcing of decadal and interdecadal oceanic variability. *Nature* **353,** 836–838 (1991).
13. Chen, F. & Ghil, M. Interdecadal variability of the thermohaline circulation and high-latitude surface fluxes. *J. Phys. Oceanogr.* **25,** 2547–2568 (1995).
14. Rahmstorf, S. Bifurcations of the Atlantic thermohaline circulation in response to changes in the hydrological cycle. *Nature* **378,** 145–149 (1995).
15. Tziperman, E., Toggweiler, R., Feliks, Y. & Bryan, K. Instability of the thermohaline circulation with respect to mixed boundary conditions: Is it really a problem for realistic models? *J. Phys. Oceanogr.* **24,** 217–232 (1994).
16. Zhang, S., Greatbatch, R. J. & Lin, C. A. A reexamination of the polar halocline catastrophe and implications for coupled ocean–atmosphere modeling. *J. Phys. Oceanogr.* **23,** 287–299 (1993).
17. Rahmstorf, S. & Willebrand, J. The role of temperature feedback in stabilizing the thermohaline circulation. *J. Phys. Oceanogr.* **25,** 787–805 (1995).
18. Manabe, S., Spelman, M. J. & Bryan, K. Transient response of a coupled ocean–atmosphere model to gradual changes of atmospheric CO_2. Part I: Annual mean response. *J. Clim.* **4,** 785–818 (1991).
19. Manabe, S. & Stouffer, R. J. Century-scale effects of increased atmospheric CO_2 on the ocean–atmosphere system. *Nature* **364,** 215–218 (1993).
20. Delworth, T., Manabe, S. & Stouffer, R. J. Interdecadal variations of the thermohaline circulation in a coupled ocean–atmosphere model. *J. Clim.* **6,** 1993–2011 (1993).
21. Manabe, S. & Stouffer, R. J. Two stable equilibria of a coupled ocean–atmosphere model. *J. Clim.* **1,** 841–866 (1988).
22. Rahmstorf, S. Climate drift in an ocean model coupled to a simple, perfectly matched atmosphere. *Clim. Dynam.* **11,** 447–458 (1996).
23. Manabe, S. & Stouffer, R. J. Simulation of abrupt climate change induced by freshwater input to the North Atlantic ocean. *Nature* **378,** 165–167 (1995).
24. Lenderink, G. & Haarsma, R. J. Variability and multiple equilibria of the thermohaline circulation associated with deep water formation. *J. Phys. Oceanogr.* **24,** 1480–1493 (1994).
25. Griffies, S. & Tziperman, E. A linear thermohaline oscillator driven by stochastic atmospheric forcing. *J. Clim.* **8,** 2440–2453 (1995).
26. Weaver, A. J. & Hughes, T. M. C. Rapid interglacial climate fluctuations driven by North Atlantic ocean circulation. *Nature* **367,** 447–450 (1994).
27. Neelin, J. D. & Dijkstra, H. A. Ocean–atmosphere interaction and the tropical climatology. Part I: the dangers of flux adjustment. *J. Clim.* **8,** 1325–1342 (1995).
28. Marotzke, J. & Stone, P. H. Atmospheric transports, the thermohaline circulation, and flux adjustments in a simple coupled model. *J. Phys. Oceanogr.* **25,** 1350–1364 (1995).
29. Schiller, A., Mikolajewicz, U. & Voss, R. The stability of the thermohaline circulation in a coupled ocean–atmosphere general circulation model. *Clim. Dynam.* (in the press).
30. Yu, E.-F., Francois, R. & Bacon, M. P. Similar rates of modern and last-glacial ocean thermohaline circulation inferred from radio-chemical data. *Nature* **379,** 689–694 (1996).
31. McManus, J. F. *et al.* High resolution climate records from the North Atlantic during the last interglacial. *Nature* **371,** 326–329 (1995).

Acknowledgements. I thank S. Manabe and R. Stouffer for allowing the use of their coupled model, and S. Griffies and R. Stouffer without whose help the completion of this work would not have been possible. This work is partially funded by the Israeli Academy of Sciences.

Correspondence should be addressed to E.T. at the Weizmann Institute of Science (e-mail: eli@beach.weizmann.ac.il).

Silent fault slip following an interplate thrust earthquake at the Japan Trench

Kosuke Heki*, Shin'ichi Miyazaki† & Hiromichi Tsuji‡

* *National Astronomical Observatory, 2–12 Hoshigaoka, Mizusawa-city, Iwate 023, Japan*
† *Geographical Survey Institute, 1 Kitasato, Tsukuba-city, Ibaraki 305, Japan*
‡ *Ministry of Construction, 2-1-3 Kasumigaseki, Chiyoda-ku, Tokyo 100, Japan*

Recent global space geodetic measurements have revealed that the velocities of tectonic plates over timescales as short as a decade[1] are consistent with models of velocities averaged over the past few million years. The slip inferred from interplate thrust earthquakes at deep sea trenches and and number of earthquakes, however, often falls short of that predicted from these observed plate convergence rates[2,3]. Here we report transient crustal movements recorded by a permanent Global Positioning System (GPS) network in northeastern Japan following a typical interplate earthquake that occurred in December 1994 at the Japan Trench. Cumulative fault slip was estimated from the postseismic displacements at the GPS points over the first year after the event, and the inferred amount of seismic moment released by the afterslip was comparable to that released in the high-speed rupture. Such seismically 'invisible' slip may therefore account for the shortage of seismic slip relative to that required by time-averaged plate velocities.

Slips associated with modern and historical interplate earthquakes at the Japan Trench (off the Sanriku coast, northeastern Japan) account for only one-fifth of the time-averaged rate of the Pacific plate subduction[2]. Kawasaki *et al.*[3] recently discovered there an 'ultra-slow earthquake' with source time of ~1 day in extensometer records and hypothesized that the deficiency is taken up by such slow processes which are difficult to detect by conventional seismometric observations. The Sanriku–Haruka–Oki earthquake (moment magnitude $M_w = 7.6$) occurred there on 28 December 1994 as a typical interplate thrust event (Fig. 1). The hypocentral depth is very shallow and the aftershock area of about 150 × 70 km (east–west × north–south) dips to the west along the boundary between the subducting slab and the overriding plate. The focal mechanism solutions indicate that major slip occurred in the central part of the aftershock area[4,5], which is consistent with the slip distribution (Fig. 1) inferred by joint inversion[6] of tsunami waveforms and coseismic displacements observed by the Japanese nationwide permanent GPS network.

This GPS network was established in October 1994 by the Geographical Survey Institute (GSI) of Japan with about 200 dual-band P-code receivers that cover most parts of Japan[7]. We analysed the data of 16 stations located in northeastern Honshu and southern Hokkaido, October 1994 to December 1995; we used release 9.28 of the GAMIT software[8] with International GPS Service for Geodynamics (IGS) precise ephemerides and Earth orientation parameters from the International Earth Rotation Service (IERS) Bulletin B. Tropospheric delays are estimated at each station in every 3-hour period. Daily horizontal site positions with respect to the Tsukuba IGS station ~500 km south of the epicentre (Fig. 1), were used to study postseismic crustal movements. Figure 2 shows the time series of three sites, Mutsu, Aomori and Kuji; the locations of these sites are shown in Fig. 1. Their coordinates change little before the earthquake (time $t = -0.2$ to 0.0 yr), then coseismic displacements are clearly seen as discontinuities at $t = 0$ (maximum displacement of 9.2 cm at Kuji). Postseismic crustal movements are characterized by steep onsets and gradual decay over $t = 0.0$ to 1.0 yr (maximum displacement of 5.8 cm after 1 year at Kuji).

Thatcher *et al.*[9] derived a viscosity of 1×10^{19} Pa s for the uppermost asthenosphere in this region, which implies that viscous relaxation governs processes only with timescales of a few tens of years or longer. We assume here that the observed postseismic crustal movements are generated by a slow afterslip somewhere on the fault plane that ruptured in the mainshock, and we rule out viscous effects. Direct field observation of the fault afterslip[10] and theoretical studies based on rate- and state-dependent friction laws[11] suggest that afterslip obeys logarithmic decay approximated by $\alpha \ln(\beta t + 1)$; this equation is a simplified form of equation (5) in ref. 11, where t is the time after an earthquake, and α and β are parameters defining overall amplitude and temporal decay, respectively. (β reflects, for example, coseismic rupture time, degree of velocity-strengthening and proportion of the stable/unstable fields; ref. 12.) We estimated α and β from GPS point horizontal displacement time series using iterative nonlinear curve-fitting techniques. We estimated α as arc parameters for individual components/sites (actually we estimated one-year cumulative displacements which are proportional to α) while β was estimated as the common global parameter because surface crustal movements would have the same

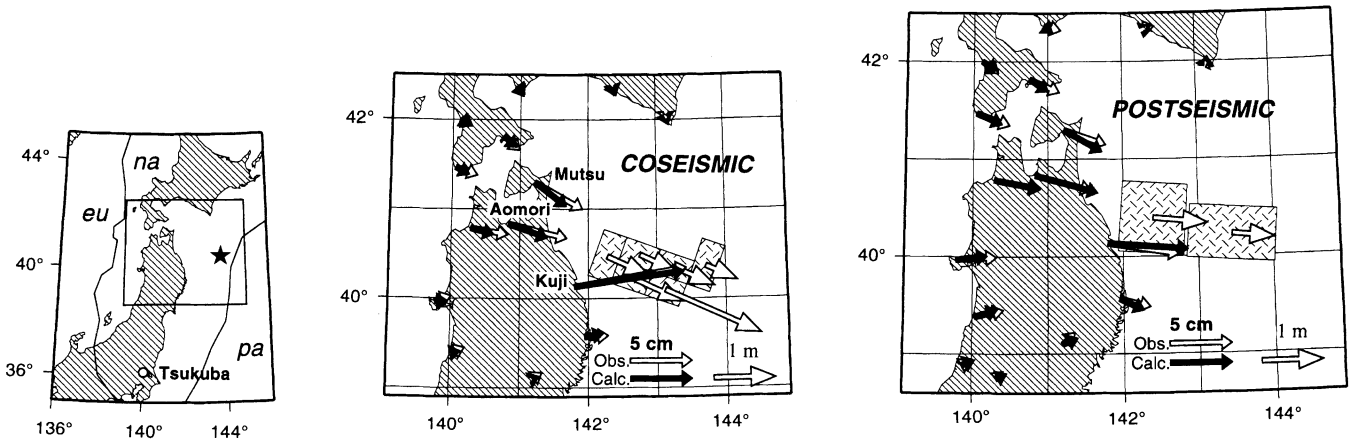

Figure 1 Left, panel showing the epicentre of the mainshock of the 28 December 1994 Sanriku-Haruka-Oki earthquake (star), plate boundaries (na, North America; eu, Eurasia; pa, Pacific), the Tsukuba GPS station (open circle), and the studied area (rectangle). The middle and right panels show respectively the co- and post-seismic crustal movements. White arrows for GPS points denote the observed horizontal movements; black arrows show the calculated movements. The 'observed' co- and post-seismic displacements were derived as discontinuities at $t = 0$ in the coordinate time series, and by fitting logarithmic decay curves to the coordinate time series over the one-year period, respectively (Fig. 2). The 'calculated' co- and post-seismic displacements were obtained by assuming the geometry/slip of the faults shown in the figure as cross-hatched rectangles/arrows, and an elastic half-space. Coseismic fault parameters are taken from ref. 6 while postseismic slips were estimated in this study. The afterslip for the eastern segment was 69.4 ± 18.9 cm towards N97.2E (strike, 185°; dip 8°; 60 × 100 km; fault centre at 40° 23′ N, 143° 45′ E; depth, 17.0 km). The afterslip for the western segment was 88.5 ± 8.0 cm towards N97.2E (strike, 185°; dip, 35°; 80 × 90 km; fault centre at 40° 39′ E, 142° 40′ E; depth, 49.8 km).

temporal decay property as the afterslip at depth. Using 3,840 measurements from 11 stations, β was estimated as $6.5 \pm 0.6\,\mathrm{yr}^{-1}$, that is, about half of the motion of the first year is achieved in the first 100 days. This is somewhat longer than reported in the strike-slip cases[11] where half of the first-year movement is often achieved in a few tens of days. We obtained a post-fit residual of 4.4 mm, a value not so different from those we usually obtain in fitting lines to the secular movements of GPS stations in Japan. Displacements of an additional five stations, farthest from the epicentre with displacements of a few millimetres, were obtained by simple linear regression.

Horizontal displacement vectors over the one-year postseismic period of the 16 GPS sites were used to derive the amount of fault slip using the dislocation theory in an elastic half-space formulated by Okada[12]. Vertical components were not used because the largest expected displacement (one-year cumulative uplift of ~1 cm at Kuji) is as small as their day-to-day repeatability. It was almost impossible to reproduce the displacement directions when using only the afterslip in the updip and/or downdip extensions of the aftershock area, so we assumed that most afterslip occurred in the same part of the rupture plane as the mainshock (although we cannot rule out minor afterslips in its downdip and/or updip extensions). We used the aftershock distribution[13] to delimit the size and the location of the faulted slip surface and divided it into two segments, the shallowly dipping eastern part and the moderately dipping western part (Fig. 1). Because GPS points exist only on one side of the fault (the land area), interparameter correlation makes it difficult to resolve detailed slip distribution by dividing it into small segments (if we split the eastern segment into two, their correlation becomes >95% and the formal errors exceed 1 metre). Slip direction could be fixed to an *a priori* value if we knew on which plate northeastern Japan resides. Because this is not the case at the moment[14], we estimated the slip direction common for the two segments, together with the inidividual slips.

The weighted root-mean-squares of the displacement after estimating these three parameters (the slip amounts of the eastern and western fault segments, and their direction) was 4.3 mm and the estimated slip direction was N97.2E (Fig. 1) with 1σ formal error of 2.6°. This deviates by ~15° (~10°) anticlockwise from the direction that the NUVEL1 model[15] predicts for the North American (Eurasian)–Pacific plate convergence there. The estimated fault slips were 88.5 ± 8.0 cm and 69.4 ± 18.9 cm for the western and the eastern segments, respectively. Assuming[6] a shear modulus of 40 GPa, they correspond to the seismic moment of 4.2×10^{20} N m, larger than the total moments released by the aftershocks[13] by an order of magnitude, indicating that the slip was largely aseismic. Fit is relatively poor (that is, observed eastward velocities are too large) for the stations along the Japan Sea coast. The amount and the sense of these misfits seem consistent with the interseismic east–west shortening in this region[16] because the easternmost sites of the network are situated at similar distances from the trench axis to Tsukuba, the fixed reference. If we eliminate interseismic east–west shortening of $3 \times 10^{-8}\,\mathrm{yr}^{-1}$ (ref. [16]) fixing Kuji, the weighted root-mean-squares of the residuals decreases to 3.5 mm. This, however, does not change the estimated seismic moment more than a few per cent.

In October 1994, the Hokkaido–Toho–Oki earthquake[7], an 'intraplate' earthquake, occurred within the subducting slab ~400 km northeast of the Sanriku–Haruka–Oki earthquake. Although it brought larger coseismic movements of GPS points in Hokkaido[7], our preliminary analyses show that the postseismic movements are insignificant. This suggests that the distinct afterslip was peculiar to 'interplate' earthquakes, and attributable to the nature of the fault surface such as the existence of unconsolidated sediments. Pacheco *et al.*[2] supposed that convergent plate interfaces are made up of three parts, patches of unstable (velocity-weakening) field (that is, asperities), stable (velocity-strengthening) field and compliant (conditionally stable) field, and earthquakes nucleate only in the first field. The unstable field may be dominant in 'strongly coupled' subduction zones such as Chile, but exist only as small patches in 'weakly coupled' zones such as Sanriku where seismic coupling coefficients are small. In the present case, the major part of the after slip seems to have occurred in the same part as the coseismic rupture, in contrast with the two cases in Chile where afterslips were suggested in the updip[17] or downdip[18] extensions. This case might be understood as a sequence with the instantaneous coseismic slip 'mainly' in the unstable field (that is, it might have propagated into the stable field), and the postseismic slow fault

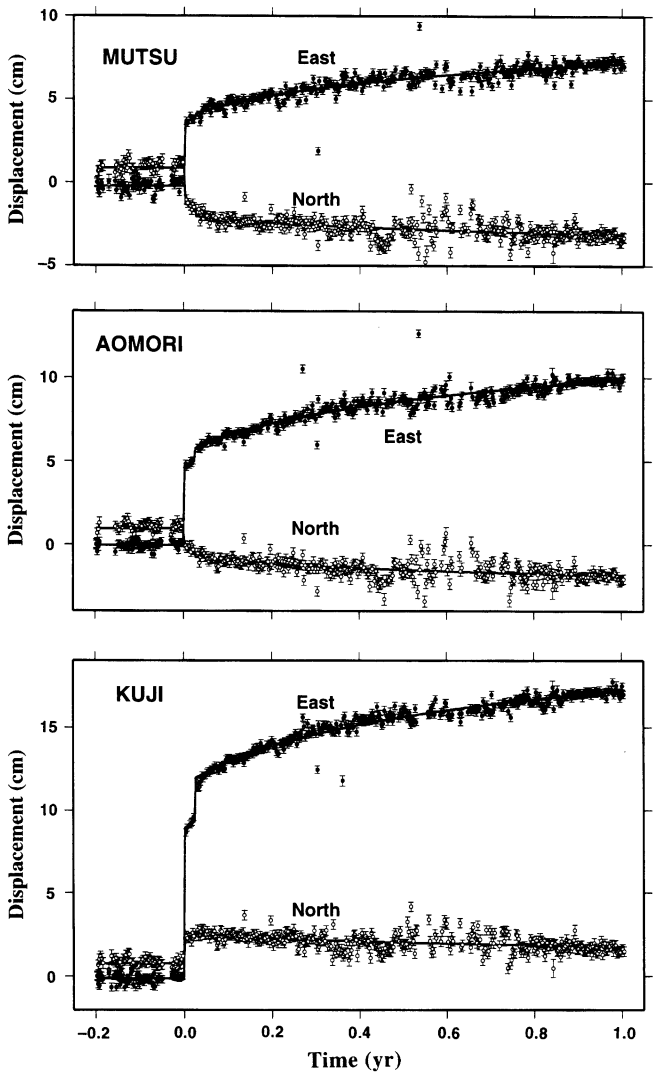

Figure 2 Horizontal coordinate time series before and after the 1994 Sanriku-Haruka-Oki earthquake observed at the three GPS points, Mutsu, Aomori and Kuji (Fig. 1). Horizontal axes show the time in years after the earthquake, and coordinates in the vertical axes are taken relative to arbitrary values. Open and filled circles denote north and east components, respectively. Thick black lines are the model curves (stationary for $t < 0$, logarithmic decay for $t > 0$, discontinuity at $t = 0.0$). The largest aftershock (surface-wave magnitude $M_s = 6.9$) occurred ~9.5 days after the mainshock ($t \approx 0.03$) and these stations underwent horizontal coseismic displacements of about 2.6 cm, 0.9 cm and 0.7 cm, respectively, which were removed from the curve-fitting processes by estimating additional discontinuities. No sizeable coseismic displacements were found for other smaller aftershocks (Japan Meteorological Agency counted 22 aftershocks with $M > 5$; ref. 13).

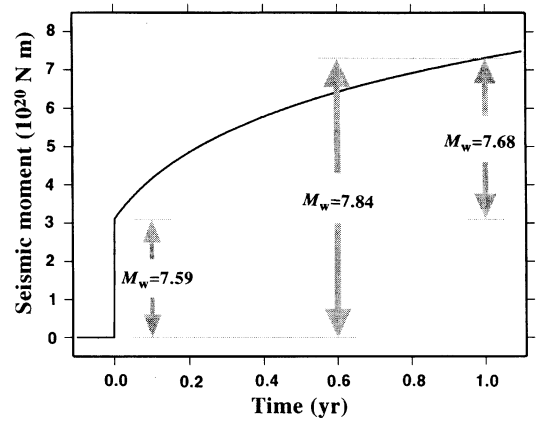

Figure 3 Coseismic and postseismic moment release curve inferred for the 1994 Sanriku-Haruka-Oki earthquake sequence. Moment magnitudes (M_w) equivalent to the coseismically released seismic moments, and the total moment after one year, are indicated.

movement 'mainly' in the compliant/stable fields with complementary slip distribution that equalizes the total slip throughout the fault plane. Although the present GPS network does not have enough resolution to derive detailed postseismic slip distribution, we can notice some differences between the coseismic and postseismic movements in Fig. 1; for example, the coseismic displacement of Kuji is more than twice as large as Aomori and deflected anticlockwise by ~30° from it, while postseismic displacement vectors of these points are more alike. This suggests that the afterslip distribution is relatively even throughout the fault surface while the coseismic slip concentrates more or less in a small central part corresponding to the asperity.

Postseismic moment release of 4.2×10^{20} N m corresponds to $M_w = 7.7$, larger than the coseismic release of 3.1×10^{20} N m ($M_w = 7.6$) suggested by the slip distribution of ref. 6. The whole sequence corresponds to an earthquake of $M_w = 7.8$ with a source time of one year (Fig. 3), much longer than ~1 day found in the same region[3], and ~1 week found in California[19]. Together with the 1992 ultra-slow earthquake[3], and the 1896 Tsunami earthquake[20], this case shows that it is not unusual in this region for a slow fault slip to follow a brittle fracture. Small seismic coupling coefficients found worldwide in deep sea trenches[2] suggest that interplate thrust earthquakes have an aspect invisible to conventional seismometric observations. Geodetic measurements of crustal deformation (especially those by GPS with sufficient temporal and spatial coverage/density) will be important in understanding interplate thrust earthquakes over a wide range of timescales and, above all, in allowing proper seismic hazard assessments based on seismic moment budget. □

Received 11 November 1996; accepted 14 February 1997.

1. Heki, K. Horizontal and vertical crustal movements from three-dimensional very long baseline interferometry kinematic reference frame: implication for the reversal timescale revision. *J. Geophys. Res.* **101,** 3187–3198 (1996).
2. Pacheco, J. F., Sykes, L. R. & Scholz, C. H. Nature of seismic coupling along simple plate boundaries of the subduction type. *J. Geophys. Res.* **98,** 14133–14159 (1993).
3. Kawasaki, I. *et al.* The 1992 Sanriku-Oki, Japan, ultra-slow earthquake. *J. Phys. Earth* **43,** 105–116 (1995).
4. Sato, T., Imanishi, K. & Kosuga, M. Three-stage rupture process of the 28 December 1994 Sanriku-oki earthquake. *Geophys. Res. Lett.* **23,** 33–36 (1996).
5. Nishimura, T., Nakahara, H., Sato, H. & Ohtake, M. Source process of the 1994 far east off Sanriku earthquake, Japan, as inferred from a broad-band seismogram. *Tohoku Geophys. J.* **34,** 121–134 (1996).
6. Tanioka, Y., Ruff, L. & Satake, K. The Sanriku-oki, Japan, earthquake of December 28, 1994 (M_w 7.7): rupture of a different asperity from a previous earthquake. *Geophys. Res. Lett.* **23,** 1465–1468 (1996).
7. Tsuji, H., Hatanaka, Y., Sagiya, T. & Hashimoto, M. Coseismic crustal deformation from the 1994 Hokkaido-Toho-Oki earthquake monitored by a nationwide continuous GPS array in Japan. *Geophys. Res. Lett.* **22,** 1669–1672 (1995).
8. Dong, D. & Bock, Y. Global Positioning System network analysis with phase ambiguity resolution applied to crustal deformation studies in California. *J. Geophys. Res.* **94,** 3949–3966 (1989).
9. Thatcher, W., Matsuda, T., Kato, T. & Rundle, J. B. Lithospheric loading by the 1896 Riku-u earthquake, Northern Japan: implications for plate flexure and asthenospheric rheology. *J. Geophys. Res.* **85,** 6429–6435 (1980).
10. Bucknam, R. C., Plafker, G. & Sharp, R. V. Fault movement (afterslip) following the Guatemala earthquake of February 4, 1976. *Geology* **6,** 170–173 (1978).
11. Marone, C. J., Scholtz, C. H. & Bilham, R. On the mechanics of earthquake afterslip. *J. Geophys. Res.* **96,** 8441–8452 (1991).
12. Okada, Y. Internal deformation due to shear and tensile faults in a half-space. *Bull. Seismol. Soc. Am.*

82, 1018–1040 (1992).
13. Sendai District Meteorological Observatory, Japan Meteorological Agency *The 1994 Far Off Sanriku Earthquake (December 28, M7.5)*. 75–83 (Rep. 54, Coordinating Committee for Earthq. Pred., Tsukuba-city, Japan, 1995).
14. Seno, T., Sakurai, T. & Stein, S. Can the Okhotsk plate be discriminated from the North American plate? *J. Geophys. Res.* **101,** 11305–11315 (1996).
15. DeMets, C., Gordon, R. G., Argus, D. F. & Stein, S. Current plate motions. *Geophys. J. Int.* **101,** 425–478 (1990).
16. Sheng-Tu, B. & Holts, W. E. Interseismic horizontal deformation in northern Honshu and its relationship with the subduction of the Pacific plate in the Japan trench. *Geophys. Res. Lett.* **22,** 3103–3106 (1996).
17. Barrientos, S. E. Dual seismogenic behavior: the 1985 Central Chile earthquake. *Geophys. Res. Lett.* **22,** 3541–3544 (1995).
18. Barrientos, S. E., Plafker, G. & Lorca, E. Postseismic coastal uplift in southern Chile. *Geophys. Res. Lett.* **19,** 701–704 (1992).
19. Linde, A. T., Gladwin, M. T., Johnston, M. J. S., Gwyther, R. L. & Bilham, R. G. A slow earthquake sequence on the San Andreas fault. *Nature* **383,** 65–68 (1996).
20. Tanioka, Y. & Satake, K. Fault parameters of the 1896 Sanriku tsunami earthquake estimated from tsunami numerical modeling. *Geophys. Res. Lett.* **23,** 1549–1552 (1996).

Acknowledgements. We thank N. Kato for comments; A. Linde and P. Segall for critical reviews; and GSI staff for maintaining the GRAPES GPS network.

Correspondence should be addressed to K.H. (e-mail: heki@miz.nao.ac.jp)

Compression of visual space before saccades

John Ross*, M. Concetta Morrone† & David C. Burr†‡

* *Department of Psychology, Vision Laboratory, University of Western Australia, Nedlands, Western Australia 6907, Australia*
† *Istituto di Neurofisiologia del CNR, Pisa 56127, Italy*
‡ *Department of Psychology, Università di Roma, 'La Sapienza', Via dei Marsi 78, Rome 00185, Italy*

Saccadic eye movements, in which the eye moves rapidly between two resting positions, shift the position of our retinal images. If our perception of the world is to remain stable, the visual directions associated with retinal sites, and others they report to, must be updated to compensate for changes in the point of gaze. It has long been suspected that this compensation is achieved by a uniform shift of coordinates driven by an extra-retinal position signal[1–3], although some consider this to be unnecessary[4–6]. Considerable effort has been devoted to a search for such a signal and to measuring its time course and accuracy. Here, by using multiple as well as single targets under normal viewing conditions, we show that changes in apparent visual direction anticipate saccades and are not of the same size, or even in the same direction, for all parts of the visual field. We also show that there is a compression of visual space sufficient to reduce the spacing and even the apparent number of pattern elements. The results are in part consistent with electrophysiological findings of anticipatory shifts in the receptive fields of neurons in parietal cortex[7] and superior colliculi[8].

For most experiments, observers made 20° left-to-right saccades in a dimly lit room from a fixation point F_0 (at $-10°$) on an otherwise featureless red screen, to a target F_1 presented at $+10°$ after a ready signal. Green equiluminant vertical bars were briefly flashed at various positions, and observers reported their location with reference to a ruler that appeared on the screen shortly after the end of each saccade. The results in Fig. 1 show that bars displayed at physical positions of either 0 or $-20°$ (squares and triangles, respectively) were systematically mislocalized in the direction of the saccade. The shift effects begin 50 ms before the saccade, rising to a maximum (about 10°) in a critical period just before the saccade onset ($-25 < t < 0$ ms). After the saccade had finished, localization of the bar was again veridical, although it now fell on a different retinal location from before. The results were quite different for bars displayed to the right of the target F_1 at $+20°$ (circles in Fig. 1). Here the apparent position was displaced against the direction of saccades before the eye movement. The apparent length of the long bars (50°) did not change significantly under any condition (data not shown). The continuous curves in Fig. 1 and in all other figures come from the simple model described in Methods, which assumes a change in the origin of perceptual space from F_0 to F_1 and a perceptual compression.

Figure 2 describes the pattern of results found within the critical period, -25 to 0 ms (relative to saccade onset), for bars displayed over a wide range of spatial positions. Bars displayed to the left of F_1 were displaced in the direction of the saccade, whereas those to the right were displaced in the opposite direction, with a tendency for the data to cluster around F_0 and F_1 (dotted lines). Bars falling over a wide range (-5 to 30°) were mostly perceived near F_1, the saccade target. A similar pattern of results was observed for right–left, vertical and smaller (10°) saccades. These findings imply a compression of space within the critical interval. To confirm that the compression was real, we measured the vernier displacement of two half bars, first when spatially separated but displayed simultaneously and briefly. In this situation, the individual upper and lower bars behaved exactly like the full bars, resulting in the impression of

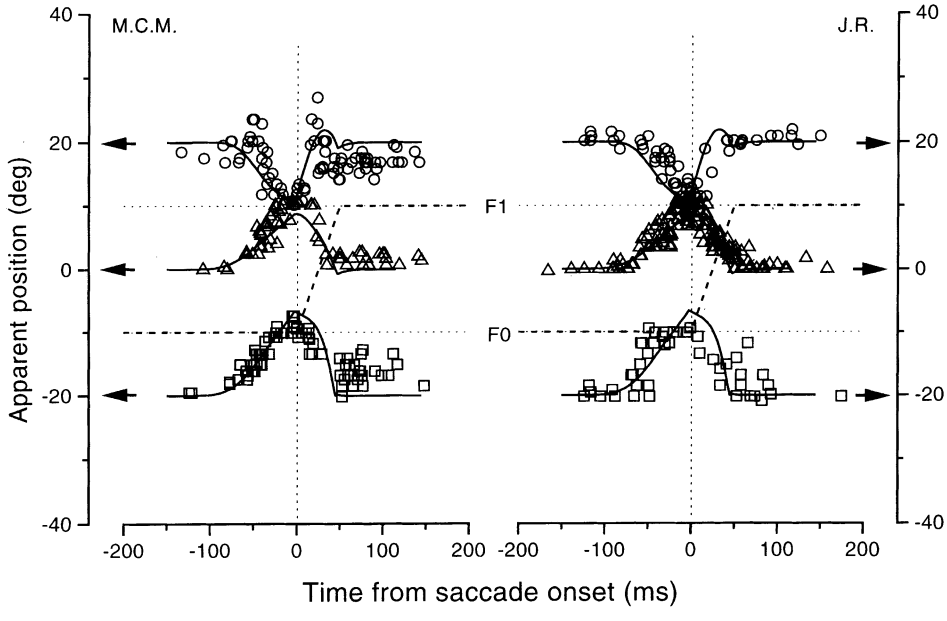

Figure 1 Apparent position of a vertical bar briefly flashed at positions $-20°$ (squares), 0° (triangles) or $+20°$ (circles), as a function of time relative to saccade onset. Each point represents a single observation. Saccades from F_0 to F_1 are indicated by the dashed line. The solid curves are simulations from the model described in Methods. Similar results have been obtained with 6 other observers, all initially naive of the aims of the experiment.